Remote sensing and on-farm experiments for determining in-season nitrogen rates in winter wheat – Options for implementation, model accuracy and remaining challenges

K. Piikki [a,*], M. Söderström [a], H. Stadig [b]

[a] Department of Soil & Environment, Swedish University of Agricultural Sciences (SLU), P.O Box 234, SE-53223 Skara, Sweden
[b] The Rural Economy and Agricultural Societies (Hushållningssällskapet), Järnvägsgatan 18, SE-53230 Skara, Sweden

A B S T R A C T

Optimised nitrogen (N) fertilisation can be used to increase farm profits, to realise the achievement of quality goals for produce, and to reduce environmental risks in the form of leaching and/or volatilisation of N compounds from the fields. This study examined options and challenges for remote sensing-based variable rate supplemental N fertilisation in winter wheat (*Triticum aestivum* L.). The models were based on data from ten field trials conducted in different regions across Sweden over three years. A two-step approach for modelling optimal N rates, suitable for practical implementation in precision agriculture, was developed and evaluated. The expected accuracies for new sites and years were assessed by leave-one-entire-trial-out cross-validation. In a first step, the average N rate was modelled from site-specific information, including data that can be obtained from on-farm experiments, i.e. N uptake in plots without N fertilisation (zero-plots) and N uptake in plots with non-limiting N supply (max-plots). In the second step, additions or subtractions from this average N rate was modelled based on vegetation indices (VIs) mapped by remote sensing. Mean absolute error of the best prediction was 14 kg N ha^{-1}. In a practical application, however, there will be additional uncertainty from several sources, e.g. uncertainty in the assessment of yield potential. The best mean N rate model was based on geographical region, cultivar, N uptake in zero-plots and yield potential, while the best model of relative N rate within the field used a new multispectral index ($d_{75}r_6$), which was designed to give a standardized measure of the steepness of the red edge of reflectance of a crop canopy spectrum. Several other multispectral VIs also performed well but red-green-blue indices were less useful. We conclude that remote sensing (to capture within-field spatial variation patterns), on-farm experiments (to determine the field mean N rate), and the farmers' experience and knowledge on local conditions (e.g. to assess the yield potential), is a useful combination of information sources in decision support systems for variable rate application of N. Options and remaining research needs for the setup of such a system are discussed.

1. Introduction

Food production needs to increase significantly in coming decades, but global cropland area is finite and environmental impacts must be minimised (FAO, 2017). Thus, appropriate methods are needed to achieve *sustainable intensification* (SI; see definition by Pretty and Bharucha, 2014) of agricultural production. Improving *fertiliser use efficiency* (see definition by FAO, 2019) for nitrogen (N) and other plant nutrients is essential for SI, since crop production has major impacts on the global cycles of these macronutrients. On global scale, nitrogen (N) use efficiency in cereal production is estimated to be 33% (Raun and Johnson,

1999). One of many measures to improve SI and nutrient use efficiency is to tailor fertiliser rates to local and current needs, such that yield potential is exploited, while risks of nutrient losses by leaching or volatilisation are minimised (European Parliament, 2019; IPCC, 2019). This is the core of the concepts *precision agriculture* (see definition by International Society of Precision Agriculture, 2018) and site-specific fertilisation. Prerequisites for efficient adaptation of fertiliser rates to local and current needs in mechanised production are that: *i)* relevant biophysical conditions can be mapped or measured on-the-go at an appropriate scale; *ii)* collected data can be integrated with agronomic knowledge and translated into site-specific optimal fertiliser rates; *iii)*

infrastructure is in place for functional data flow from data acquisition to actual use of the data in the field; and *iv*) there are no major hindrances, such as lack of adequate machinery, lack of awareness among farmers and advisory officers, too high cost or too demanding procedures, to wider adoption of variable rate application (VRA). This study examined supplementary fertilisation of N in winter wheat (*Triticum aestivum* L.) in Sweden.

1.1. Current methods to adapt N fertilisation in winter wheat

Current methods to adapt N fertilisation in winter wheat include split doses (for temporal optimization) and VRA of the final dose (for spatial optimization). In Sweden, the first N dose is typically given at around growth stage DC21–24 on the Zadoks scale (Zadoks et al., 1974), the main dose at around DC31 and the third dose at DC37–45, with possibly also a later dose. Various tools are available for adjustment of these N doses, especially later supplemental doses: e.g. leaf colour charts, handheld crop canopy reflectance sensors or leaf fluorescence or transmittance sensors, used in combination with information on preceding crop, soil organic matter content and expected yield (Ali et al., 2017). Supplemental N rate can also be adjusted on-the-go using a tractor-mounted crop canopy sensor (Raun et al., 2001; Reusch, 2003). Alternatively, a prescription map for variable N rate can be prepared using an unmanned aerial vehicle (UAV) or satellite-based decision support system (DSS) (Söderström et al., 2017; Vizzari et al., 2019). A key issue in determining optimal supplemental N rates is that empirical models linking the proximally or remotely sensed crop canopy reflectance data to the crop N status are not universal, but sensitive to e.g. the developmental stage of the crop (e.g. Chen, 2015). Therefore, local and current information, e.g. from on-farm experiments (OFE; Lacoste et al., 2022) or targeted crop canopy measurements of actual N status (Nutini et al., 2018, 2021) can be useful in an operational context. To support decisions on supplemental N rate for a farm, field or management zone, some farmers use miniature OFEs, with zero-plots (no N fertilisation) and sometimes also max-plots (sufficient N applied to ensure N is not limiting for crop growth). These plots indicate the current-year level of soil N supply and yield potential, respectively (e.g. Raun et al., 2001). Adaptation of rates is now widely used in the field, e.g. in 2021 an estimated 40–50% of the Swedish winter wheat acreage was fertilised with a variable N rate using tractor-mounted N sensors or satellite-image based DSS (unpublished statistics from Yara AB, Malmö, Sweden; unpublished survey by Federation of Swedish Farmers LRF, 2020).

1.2. Remote sensing-based DSS

Satellite-based DSS is an efficient means to provide decision support for VRA of N at a broad scale (Alshihabi et al., 2019). The Sentinel-2 satellites collect reflectance data every 2–5 days depending on latitude (ESA; Paris, France). Several DSS already use these free data for deriving nitrogen VRA prescription files or maps (Vizzari et al., 2019). Similar functionality exists in DSS based on images collected by UAVs (e.g. Solvi.ag; Solvi AB, Gothenburg, Sweden). The DSSs constitute an efficient data flow from acquisition to the end-use in the tractor, but agronomic recommendations based on the remote sensing data (absolute N rates) are still lacking. There are different benefits and drawbacks with different remote sensing platforms. Sentinel-2 data are free but may suffer from gaps in time series of useful images due to clouds, while UAV data collection may be associated with costs (both hardware and software). UAV-based vegetation index (VI) mapping may also be considered too time consuming, for a time critical action like N topdressing, during a busy period.

1.3. A new way of developing the necessary recommendations

Our overall aim was to develop models that are applicable in remote-sensing based DSSs (satellite or UAV), but as the trial plots were too small to be linked directly with Sentinel-2 data, the remote sensing of field trials to collect data for model development and evaluation was done by UAV. Relevant Sentinel-2 bands have a spatial resolution of 10 or 20 m, whereas N fertilisation plots in Swedish crop field trials are often about 2 m × 10 m. There are multispectral UAV cameras available with bands that are spectrally identical to those of the Sentinel-2 satellites (in the spectral range 400–900 nm) (Nocerino et al., 2017). This makes it possible to collect reflectance data corresponding to Sentinel-2 data, but with sufficiently high spatial resolution to identify individual plots in field trials. This opens up new possibilities; models based on UAV measurements in field trials can be applied on satellite data in DSSs, although direct transfer of models can be challenging (e.g. Wolters et al., 2022).

1.4. Aim and scope

Open algorithms can facilitate wide adoption of VRA for supplemental N fertilisation to grain crops. The specific objective in this study was to develop and evaluate models to translate remotely collected crop canopy reflectance data into directly applicable N rate maps for supplemental N fertilisation in winter wheat (around stage DC37). The hypotheses were that:

- optimal average supplemental N rate could be modelled with good enough accuracy for practical use based on combinations of the following local predictors: yield potential, cultivar, geographic region and N status in on-farm trial plots.
- optimal relative supplemental N rate, i.e the N rate to add to or subtract from the average rate, could be modelled from different vegetation indices to take current crop N status into account.
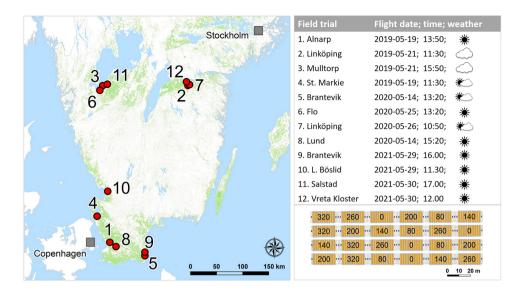
2. Materials and methods

2.1. Field trials

Data were collected over three years (2019–2021) in a Swedish field trial series (code L7–150) testing six nitrogen rates in ten winter wheat cultivars at growth stage DC37 in four trials per year. Dates and site locations are shown in Fig. 1. The trials were located within the main agricultural districts across southern Sweden. Cambisols dominate the whole area and the field trials were located in areas with soils mostly classified as silty clay, silty clay loam and clay (Piikki and Söderström, 2019). The climate is classified as Köppen region Dfb in the northeast whereas the west and south is Cfb (Kottek et al., 2006). Trial design was an orthogonal combination of 10 cultivars and six N levels (0, 80, 140, 200, 260 and 320 kg N ha^{-1} in total, of which 25% applied at tillering (DC21–24), 50% around beginning of stem elongation (DC31), and 25% just after the flag leaf was visible (DC37)). All treatments had four replicates. The trial plots were approximately 2 m × 10 m. The set of cultivars tested changed each year, but five cultivars (Etana, Julius, Hallfreda, Informer, RGT Reform) were used in all three years of the present study. Trial plans and agronomic data are available via the Nordic Field Trial System (https://nfts.dlbr.dk/). Data from the same trials (2019–2020) have been used previously by Söderström et al. (2021) for remote sensing-based yield mapping at DC69, and by Wolters et al. (2022) for modelling of crude protein content, also at DC69.

2.2. UAV-based multispectral data collection

For data collection, we used a MAIA-S2 camera (Eoptis Srl, Trento, Italy) mounted in a fixed position on a custom-built octocopter (Explorian-8; Pitchup, Gothenburg, Sweden). This camera records light in nine spectral bands with the same widths and midpoint wavelengths as bands 1–8 and 8A of the Sentinel-2 satellites (European Space Agency, Paris, France), nomenclature used for the MAIA-S2 bands in this study. The midpoint wavelength of the nine MAIA-S2 bands is 453, 490, 560,

Fig. 1. Location of the 12 field trial sites in the main agricultural districts (green areas) in southern Sweden. All unmanned aerial vehicle (UAV) flights were carried out at Zadoks growth stage DC37. Flight date (yyyy-mm-dd), approximate take-off time (local time hh:mm) and weather are shown in the upper right panel. The lower right panel shows an example of trial design, where the numbers indicate the treatment (total N fertilisation rate in kg ha^{-1}).

665, 705, 740, 783, 842 and 865 nm, respectively. One image per band was collected, at frequency 1 Hz, 80 m above ground level and flight speed 5 m s^{-1}. The route was planned using the UGCS ground control software (SPH Engineering, Riga, Latvia) so that the images overlapped by at least 80% along and between flight lines. Each flight took around 10 min and was carried out in as uniform light conditions as possible, e. g. avoiding cloud shadows. Flight dates varied somewhat depending on differences in crop development at the trial sites (Fig. 1). For practical reasons, time of day also differed between the flights, with sun elevation varying between 35 and 53 degrees (based on https://www.suncalc. org).

Before each flight, five 50 cm × 50 cm near-lambertian reflectance plates with known reflectances (2%, 9%, 23%, 44% and 75%; Mosaic Mill Oy, Vantaa, Finland) were placed along each of the short edges of the trial. When necessary, these plates were placed on racks to avoid shading by the crop.

2.3. Reflectance data preparation

2.3.1. Geometric correction by test image
Images were acquired in RAW 12-bit format by the sensor. Nine-band images (tiff) were generated using the image-processing software supplied with the MAIA camera (MultiCam Sticher Pro). The software performs spatial co-registration of the different bands, as well as geometric and radiometric corrections. The UAV was equipped with an incoming light sensor (ILS) that continuously recorded ambient light for each band of the camera, data used by the software for radiometric correction.

2.3.2. Mosaicking
The geometrically corrected images were stitched to orthomosaic raster images by the Solvi web application (https://solvi.ag; Solvi AB, Gothenburg, Sweden). Polygons of the plots were generated in the Solvi application, and all data were downloaded and further processed in ArcGIS Desktop (version 10.8; ESRI Inc., Redlands, CA, USA). The median digital number (DN) of all raster cells within each trial plot (avoiding approximately 0.2–0.3 m along the edges of the plots) was extracted, as was that for all reflectance panels.

2.3.3. Spectral correction by reflectance plates
Linear regression models between known panel reflectance values

(ρ_{panel}) and the digital numbers extracted from the mosaics (DN_{panel}) (Eq. 1) were used to calibrate the trial plot reflectance model. The linear regression models for calibration were parameterised for each trial and reflectance band.

$$\rho_{panel} = a \times DN_{panel} + b \tag{1}$$

2.4. Data cleaning

There were problems with some of the data collected. Data from two of the 12 trials had to be omitted, because of abnormal soil N supply at one site (zero-plot grain yield of 10 tonnes ha^{-1}; Alnarp 2019) and unrealistic reflectance values at another site (Mulltorp 2019). In addition, a few individual plots had to be omitted because of partial cloud shadows during the flight, erroneous treatments (cultivar or N rate not according to trial plan) or missing agronomic data. No entire treatment (N rate × cultivar combination) was discarded. In the few cases of discarded plots, treatment median values were based on fewer than four replicates. The remaining dataset consisted of median values for 300 individual treatments (six N rates × five cultivars × 10 trials). This data cleaning was performed before any data analysis was conducted.

2.5. Modelling setup and nomenclature

The modelling of optimal supplemental N rate was split into two steps on different scales. In the first step, the trial average N rate was modelled and in the second step, the optimal relative supplemental N rate in four realistic N treatments was modelled (larger or smaller N rate than the average). The modelling in the study was designed to be transferable to practical use in variable-rate application of N in precision agriculture. In the present study, field trials represent fields, and trial treatments (median of four replicates) represent variation within the field. The treatments with minimum (0 kg N ha^{-1}) and maximum (320 kg N ha^{-1}) represent OFE plots in the field (zero-plot and max-plots). The motivation for using a two-step approach, and only use remote sensing data for the second step, is primarily that absolute models would be more sensitive to developmental stage of image acquisition. In a practical application, the second step can be based on data from either satellite or UAV platforms. In order to evaluate how well the models performed at new sites, leave-one-entire-trial-out cross-validation was used instead of conventional leave-one-observation-out cross-validation. A final model was then parameterised, using all data

for parameterisation (no trial left out). The terms used in following sections are summarized in Table 1.

2.6. Nitrogen-response modelling

Yield (kg grain ha^{-1}; 15% water content) was modelled as a function of total N fertilisation rate (kg N ha^{-1}) over the season (Eq. (2)). Models were parameterised for each trial and cultivar. A sigmoidal function, asymptotically approaching a maximum, was chosen over the commonly used second-grade or third-grade polynomials, as a monotone increasing function was considered a better representation of the crop yield response to the supply of plant-available N. Initial tests of various univariate functions (not reported) showed that this function fitted the collected data well.

$$y = a - \frac{a - b}{1 + cx^2} \qquad (2)$$

In Eq. (2), y is Y$_{treat}$, x is NR$_{tot\_treat}$ and a, b and c are the model parameters. The parameters were estimated by the least square method (nls function in the stats package of the R software environment; R Core Team, 2021).

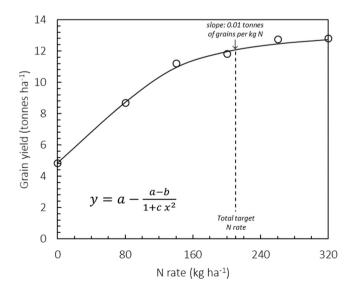## 2.7. Determination of total target N rate

The optimal N rate (i.e the target total N rate; NR$_{target\_trial}$) is often determined as the N rate where the yield increase in response to increasing N rate gives a net economic return of zero (e.g. Piikki and Stenberg, 2017). The target N rate is then the N rate at which the price of the extra harvested grain is equal to the cost of the extra N fertiliser, i.e. when the derivative of the dose-response function (Eq. (2)) equals the price ratio of the grain and the fertiliser N. In the present study, NR$_{target\_trial}$ was instead determined as the N rate for which the yield increase was 10 kg per kg N, i.e. where the derivative of y in Eq. (2) (y'; Eq. (3)) equals 10 kg grain per kg N.

$$y' = \frac{2c(b - a)x}{c^2(x^4) + 2cx^2 + 1} \qquad (3)$$

There were two reasons for choosing a price-independent approach: *i*) the price ratio lacks biological relevance, and *ii*) prices change over time. In addition, Delin and Stenberg (2012) showed that loss of N to the environment is very low as long as the effect of adding 1 kg N results in at least 10 kg grain. Boundary conditions were applied as follows: computed NR$_{target\_trial}$ values < 0 were set to zero and values > 320 kg N ha^{-1} were set to 320 kg N ha^{-1}. A graph showing how NR$_{target\_trial}$ was computed is presented in Fig. 2.

2.8. Determination of supplemental N rate

The supplemental N rate (NR$_{sup\_treat}$) was determined as the difference between the target N rate for the trial and cultivar in question, and the amount of N applied in the N treatment before DC37 (NR$_{early\_treat}$).

Table 1
Nomenclature used in the modelling. VI = vegetation index.

Term	Abbreviation	Explanation
N uptake in a zero-plot	Nup$_{zero}$	In the modelling, it is the N uptake in the trial treatment without N fertilisation. In a practical application, it is the N uptake in an on-farm trial plot without N fertilisation.
N uptake in a max-plot	Nup$_{max}$	In the modelling, it is the N uptake in the highest N treatment of a trial. In a practical application, it is the N uptake in an on-farm trial plot without N limitation.
Yield potential	Y$_{pot}$	In the modelling, it is the yield in the highest N treatment of a trial. In a practical application, it is the potential yield, if there is no N limitation. Note that this is not necessarily the same as the yield at target N rate.
Yield in a trial treatment	Y$_{treat}$	The yield in an N treatment in a trial.
Total N rate in a trial treatment	NR$_{tot\_treat}$	The total N rate applied during a season in an N treatment in a trial.
Target total N rate	NR$_{target\_trial}$	The optimal total N rate to apply during the season. It is *determined* from the production function (yield as a function of total N rate over the season). It is *modelled* as a function of combinations of cultivar, region, Nup$_{zero}$, Nup$_{max}$ and Y.
Early N rate in a trial treatment	NR$_{early\_treat}$	The N rate in a trial treatment or a pixel in a map of a field or a zone (practical application) applied before supplemental fertilisation in DC 37.
Supplemental mean N rate	NR$_{sup\_treat}$	In the modelling, it is the supplemental N rate in an N treatment of a trial. In a practical application, it is a pixel in a map of a field or a zone. It is modelled from ancillary data (e.g. region, cultivar, Ypot, Nup$_{zero}$ and Nup$_{max}$
Supplemental relative N rate	NR$_{sup\_treat\_rel}$	In the modelling, it is the supplemental N rate in a treatment relative to the mean supplemental N rate of the trial. In a practical application, it is the supplemental N rate in a pixel relative to the mean supplemental N rate of the field or the management zone. This is the N rate (positive or negative) to add to the supplemental mean N rate. It is modelled from vegetation indices.
VI at the time for supplemental fertilisation	VI$_{sup\_treat}$	In the modelling, it is the VI in an N treatment of a trial. In a practical application, it is the Vi in a pixel in a map of a field or a zone.
Relative VI at the time for supplemental fertilisation	VI$_{sup\_treat\_rel}$	In the modelling, it is the VI in a treatment relative to the mean VI of the trial. In a practical application, it is the VI in a pixel relative to the mean VI of the field or the management zone.

Fig. 2. Example of an N response curve. A monotone increasing function (Eq. (2)) was fitted between yield and N rate for each trial and cultivar. Target total N rate was computed as the N rate where the slope of the curve equalled 10 kg grain per kg N (Eq. (3)). Data in this diagram are from the trial in Brantevik 2020, cultivar Hallfreda.

Any negative remaining supplemental N rates were set to zero. This was computed only for realistic N treatments (80, 140, 200 and 260 kg N ha^{-1}), i.e. within the range used in practice by Scandinavian farmers. The N rates given before DC37 were 60, 105, 150 and 195 kg N ha^{-1} (in treatments with total rates of 80, 140, 200 and 260 kg N ha^{-1}).

$$NR_{sup\_treat} = NR_{target\_trial} - NR_{early\_treat} \tag{4}$$

2.9. Determination of relative supplemental N rate

Relative supplemental N rate was computed for each treatment by subtracting the mean supplemental N rate of the realistic treatments for the trial and cultivar (Eq. (5)).

$$NR_{sup\_treat\_rel} = NR_{sup\_treat} - \overline{NR_{sup\_treat}} \tag{5}$$

2.10. Computation of vegetation indices

For each trial plot, we computed sixteen multispectral vegetation indices, four red-green-blue (RGB) vegetation indices, and N uptake modelled from one of the multispectral indices expected to be potentially useful predictors of remaining NR$_{sup\_treat\_rel}$ (i.e. indices sensitive to crop canopy biomass and chlorophyll content). The equations are presented in Table 2. In most cases, commonly used indices were included, but also combinations of bands chosen based on the reflectance spectra used in the study (d$_{74}$r$_6$, d$_{75}$r$_6$ and d$_{74}$r$_{56}$). In addition, an in-season N uptake (Nup) model for winter wheat developed by Wolters et al. (2021) was computed for zero- and maxplots (Nup$_{zero}$ and Nup$_{max}$).

2.11. Determination of relative vegetation index

Relative values of each vegetation index was computed for the realistic N treatments in the same way as NR$_{sup\_treat\_rel}$ was computed; the mean VI for the realistic N treatments in the trial and cultivar in question was subtracted from the VI in the N treatment (Eq. (6)):

$$VI_{sup\_treat\_rel} = VI_{sup\_treat} - \overline{VI_{sip\_treat}} \tag{6}$$

2.12. Modelling total target N rate

Total target N rate was modelled based on 31 different predictor sets (combinations of the five predictor variables: region, cultivar, Nup$_{zero}$, Nup$_{max}$ and Y$_{pot}$, where region is a categorical variable for the geographical districts (East: Linkoping and Vreta Kloster, South: Brantevik, St. Markie and Lund, and West: L. Böslid, Salstad and Flo; see Fig. 1). Models implemented in a DSS need to be robust and perform well in other locations and under other conditions than those for which they were parameterised. Wolters et al. (2022) demonstrated that simple regression models with fewer predictor variables worked better than a more complex model type using more predictor variables for robust crude protein prediction, using data from the same trials as in the present study. Guided by this, and in order to reduce the risk of overfitting and poor performance at new sites, we chose to parameterise univariate or multivariate linear regression models (Eq. (7)), where a and b are parameters and x$_1$, x$_2$, …, x$_n$ are predictors.

$$NR_{sup\_treat} = a + b_1x_1 + b_2x_2 + \ldots + b_nx_n \tag{7}$$

2.13. Modelling relative supplemental N rate

The relative supplemental N rate (NR$_{sup\_treat\_rel}$) was modelled from each of the relative vegetation indices. The model type was second-grade polynomial (Eq. (8)). In Eq. (8), *a*, *b* and *c* are model parameters.

$$NR_{sup\_treat\_rel} = a + b \times VI_{sup\_treat\_rel} + c \times VI_{sup\_treat\_rel}^2 \tag{8}$$

2.14. Computing total supplemental N rate

The total supplemental N rate, NR$_{sup\_treat,}$ for each plot was computed by Eq. (9), which was obtained by solving Eq. (5) for NR$_{sup\_treat}$. Negative NR$_{sup\_treat}$ values were set to zero.

Table 2

Vegetation indices (VIs) used as predictor variables for remaining N requirement in DC37. In the band columns, 1 indicates use of the band to compute the index. In the equations, ρ_3 denotes reflectance in band 3 (b$_3$) etc. Numbers 450, 556 etc. denote midpoint wavelength (λ_2, λ_3,., λ_{8A}) (in nm) in the multispectral camera bands. B= blue; G = green; R = red; RE = red edge; NIR = near infrared. Normalised difference index (NDI$_{mn}$)= (ρ_m-ρ_n)/(ρ_m+ρ_n).

Index	Wavelength bands								Formula	Reference / comment
	B	**G**	**R**	**RE**		**NIR**				
	490 b$_2$	560 b$_3$	665 b$_4$	705 b$_5$	740 b$_6$	783 b$_7$	843 b$_8$	865 b$_{8A}$		
Multispectral VIs										
NDVI			1				1		NDI; m= 8 and n = 4	Rouse et al. (1973)
NDRE$_{86}$					1		1		NDI; m= 8 and n = 6	Barnes et al. (2000)
NDRE$_{76}$				1	1				NDI; m= 7 and n = 6	- " -
NDRE$_{75}$				1		1			NDI; m= 7 and n = 5	- " -
ChlI				1	1				$(\rho_7/\rho_6) - 1$	Gitelson et al. (2003)
MSAVI$_2$		1					1		$0.5(2\rho_8 + 1 - sqrt((2\rho_8 + 1)^2 - 8(\rho_8 - \rho_4)))$	Qi et al. (1994)
OSAVI		1					1		$(1 + 0.16)(\rho_8 - \rho_4)/(\rho_8 + \rho_4 + 0.16)$	Huete (1988);Rondeaux et al. (1996)
REIP		1					1		$700 + 40((\rho_4 - \rho_7)/2 - \rho_5)/(\rho_6 - \rho_5)$	Guyot et al. (1988)
TCARI		1	1	1					$3((\rho_5 - \rho_4) - 0.2(\rho_5 - \rho_3)(\rho_5/\rho_4))$	Kim et al. (1994);Haboudane et al. (2002)
d$_{74}$r$_6$		1		1	1				$(\rho_7 - \rho_4)/\rho_6$	
d$_{75}$r$_6$			1	1	1				$(\rho_7 - \rho_5)/\rho_6$	
d$_{74}$r$_{56}$			1	1	1	1			$2(\rho_7 - \rho_4)/(\rho_5 + \rho_6)$	
ChlINDRE$_{75}$				1	1	1			ChlI/NDRE$_{75}$	
ChlIr$_8$				1	1	1			ChlI/ρ_8	
ChlIr$_9$				1	1			1	ChlI/ρ_{8A}	
TCOS		1	1	1			1		TCARI/OSAVI	Haboudane et al. (2002)
RGB indices										
TGI	1	1	1						$-0.5((\lambda_4 - \lambda_2)(\rho_4 - \rho_3) - (\lambda_4 - \lambda_3)(\rho_4 - \rho_2))$	Hunt et al. (2013)
NGRDI		1	1						NDI; m = 4 and n = 3	Bannari et al. (1995)
GLI	1	1	1						$(2\rho_3 - \rho_4 - \rho_2)/(2\rho_3 + \rho_4 + \rho_2)$	Louhaichi et al. (2001)
VARI	1	1	1						$(\rho_3 - \rho_4)/(\rho_3 + \rho_4 - \rho_2)$	Gitelson et al. (2002)
Canopy property										
Nup (N uptake; kg ha^{-1})				1	1				$12.44 + 199.86((\rho_7/\rho_6) - 1)$	Wolters et al. (2021)

$$NR_{sup\_treat} = NR_{sup\_treat\_rel} + \overline{NR_{sup\_treat}} \qquad (9)$$

2.15. Computing evaluation metrics

Two evaluation metrics were computed based on the leave-one-entire-trial-out cross-validation of models: the mean absolute error (MAE) and Nash-Sutcliffe modelling efficiency (E) (Nash and Sutcliffe, 1970). These are sensitive to both random and systematic errors (see e.g. Piikki et al., 2021 for a visualisation). The Nash-Sutcliffe modelling efficiency can take on values between negative infinity and one, where a value of 1 indicates a perfect fit whereas negative values indicate that the model is less accurate than a simple mean of the observed values. The metrics were computed for each predictor set in the NR_{target_trial} modelling, for each VI in the $NR_{sup\_treat\_rel}$ modelling, as well as for the subsequently determined NR_{sup_treat} values. The latter was done for all NR_{target_trial} predictor sets in combination with the best performing multispectral index and the best performing RGB index. The reason was that it can be of interest to apply models on multispectral satellite or UAV-borne cameras, and on data from simpler UAV-borne RGB cameras.

2.16. Comparing predictor importance for target N rate modelling

The reduction in MAE (ΔMAE) when a predictor was added to each of the 15 combinations of the other four predictors was used to assess its importance (Eq. (10)). Set i is any predictor set without the evaluated predictor variable.

$$\Delta MAE = MAE_{set\ i} - MAE_{set\ i\ +\ evaluated\ predictor} \qquad (10)$$

2.17. Analysis of reflectance spectra

Mean reflectance values were derived for different N rates and cultivars, and two-way analysis of variance (ANOVA) was conducted with N rate and cultivar as factors. The N rate included the four N treatments considered most representative of practice (80, 140, 200 and 260 kg N ha^{-1}). The ANOVA was conducted on treatment medians, with the 10 trials as replicates.

Correlation analysis between reflectance and N rate applied earlier in the season or supplemental N rate was carried out for eight bands of the UAV sensor (band 1 excluded since the corresponding band of the Sentinel-2 satellite is merely used for cloud detection and is not applicable for precision agricultural practices). The coefficients of determination (r^2) were plotted against the midpoint wavelengths of the bands. Note that N rate can be treated as both a categorical variable (as in ANOVA) and a continuous variable (as in correlation analysis), while NR_{sup_treat} can only be treated as a continuous variable.

3. Results

3.1. Descriptive statistics on field trial data

Mean NR_{target_trial} for the trials ranged from 112 to 222 kg N ha^{-1} (Table 3). The standard deviation of the trial mean values was 39 kg N ha^{-1}, while the standard deviation for cultivars ranged between 5 and 22 kg N ha^{-1}. Thus, the variation in NR_{target_trial} seemed to be larger between sites and years than between cultivars for the same site and year. However, the yield in zero-plots was relatively high in most trials, as was the yield in max-plots, which indicates that the field trials were carried out under relatively favourable conditions and cannot be considered representative for fields with poor soils.

3.2. Crop canopy spectra

Average reflectance spectra from multispectral measurements of the crop canopy in different N treatments and in different cultivars are presented in Fig. 3a-b. The spectral differences between crops that

Table 3

Descriptive statistics on the field trial data. Mean for all cultivars ± standard deviation between cultivars. NR_{target_trial} = target total nitrogen rate.

Site	Region	Year	Yield in zeroplot (kg ha^{-1})	Yield in maxplot (kg ha^{-1})	NR_{target_trial} (kg ha^{-1})
Linkoping	East	2019	6422 ± 482	9861 ± 488	126 ± 9
St. Markie	South	2019	4421 ± 278	8443 ± 366	112 ± 9
Linkoping	East	2020	6949 ± 401	10,637 ± 349	202 ± 19
Brantevik	South	2020	4838 ± 171	12,594 ± 437	222 ± 12
Lund	South	2020	4485 ± 362	9889 ± 253	162 ± 7
Flo	West	2020	2319 ± 91	9647 ± 348	206 ± 5
Vreta Kloster	East	2021	6468 ± 360	9108 ± 504	121 ± 7
Brantevik	South	2021	6020 ± 180	10,043 ± 583	137 ± 15
L. Böslid	West	2021	4150 ± 268	9771 ± 427	167 ± 22
Salstad	West	2021	4658 ± 216	9556 ± 530	141 ± 18

received different amounts of N followed the expected pattern, i.e. crops with higher N fertilisation rates had higher reflectance values in the NIR bands (7, 8 and 8a), lower reflectance values in the visible bands (2, 3 and 4) and a steeper reflectance slope between the two red edge (RE) bands (5 and 6). Coefficient of determination (R^2) between reflectance and the N rate applied before the spectral measurements (DC37) was highest for the NIR bands, followed by band 5 and band 3 (Fig. 3c), and the difference in reflectance between N rates was statistically significant ($p < 0.05$) for these bands (Table 4). There was a stronger correlation between reflectance and N requirement by the crop (the supplemental N rate) than between reflectance and N rate applied earlier in the season. The difference was larger in both the visible and NIR wavelength regions. The correlation coefficient between N rate and reflectance was negative for bands 2–5, while the correlation coefficient between NR_{sup_treat} and reflectance was negative for bands 6–8 and 8a (not shown).
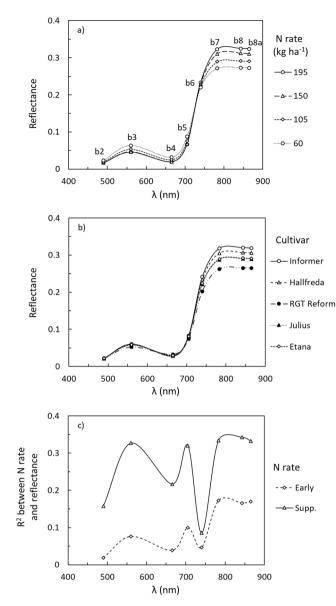
Inspection of the crop canopy in the field trials showed that the winter wheat cultivars differed in colour, leaf surface structure and canopy architecture. The difference in reflectance between cultivars was statistically significant for bands in the upper RE and NIR wavelength region (bands 6–8 and 8a). There were no statistically significant interactive effects on crop canopy reflectance between cultivar and N rate.

Fig. 3 was used as the basis for choice of VIs to be used for modelling, and to create the new proposed indices $d_{74}r_6$, $d_{75}r_6$ and $d_{74}r_{56}$ (Table 2). The lack of a strong correlation between supplemental N rate and reflectance in band 6 (close to the RE inflexion point) made this band suitable for standardising indices between trials, and it was therefore used in the denominator in these VIs.

3.3. Model performance at new sites and years

3.3.1. Optimal N rate modelling

Results from the test of different predictor sets for NR_{target_trial} modelling are presented in Table 5. The best predictions of NR_{target_trial} were based on information on region and cultivar, together with Nup_{zero} and Y_{pot} (E = 0.77, MAE = 14.4 kg N ha^{-1}). The same set but with Nup_{max} (which can be measured during the season) instead of Y_{pot} (which has to be manually assessed) performed much worse (E = 0.29, MAE = 27.3 kg N ha^{-1}), indicating that Nup_{max} is not a useful proxy for Y_{pot}. A scatter plot of predicted versus observed target total N rate values for the best-performing model is shown in Fig. 4. Model equations for four well-performing predictor sets are presented in Table S1 in Supplementary Material. Overall, adding Y_{pot} to the predictor set improved the predictions considerably (Fig. 5). However, in practical applications Y_{pot} would have to be provided by the user, from experience or possibly from some yield prediction model. In any case, it can be assumed that yield assessment early in the season is relatively uncertain. Nitrogen uptake in zero-plots (Nup_{zero}) was a useful predictor, while adding

Fig. 3. Mean reflectance spectra for a) different N rates before DC37 and b) different cultivars, and c) coefficient of determination (R2) between reflectance and N rate before DC37 (NR$_{early\_treat}$) or crop N status represented by optimal supplemental N rate (NR$_{sup\_treat}$). Symbols represent midpoint wavelength (λ) of the MAIA-S2 multispectral camera bands and labels (in a) denote corresponding band of the Sentinel-2 satellite.

Table 4
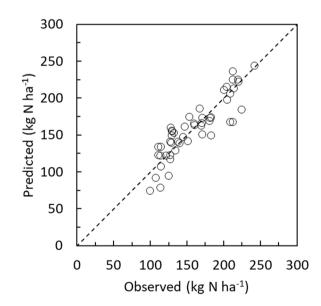Probability (p)-values and level of statistical significance (ns $p \geq 0.05$; *$p < 0.05$; **$p < 0.01$; ***$p < 0.001$) in two-way analysis of variance (ANOVA) with N rate and cultivar as factors. The 10 trials were considered replicates. Zero-plots and max-plots were excluded from all analyses.

Band	N rate		Cultivar	
2	3.5E-01	(ns)	9.6E-01	(ns)
3	3.7E-03	(**)	4.7E-01	(ns)
4	9.1E-02	(ns)	7.7E-01	(ns)
5	5.8E-04	(***)	3.9E-01	(ns)
6	1.4E-02	(*)	2.1E-14	(***)
7	1.8E-07	(***)	5.6E-08	(***)
8	4.8E-07	(***)	2.6E-07	(***)
8a	3.0E-07	(***)	1.7E-07	(***)

Table 5
Evaluation metrics for the leave-one-entire-trial-out cross-validation of target total N rate models for 31 predictor sets (combination of region, cultivar, N uptake in zero-plots (Nup$_{zero}$), N uptake in max-plots (Nup$_{max}$), and yield potential (Y$_{pot}$)). The number 1 indicates inclusion in the predictor set. E = Nash-Sutcliffe modelling efficiency; MAE = mean absolute error.

Set	Region	Cultivar	Nup$_{zero}$	Nup$_{max}$	Y$_{pot}$	E	MAE (kg N ha^{-1})
1	1					< 0	44.9
2		1				< 0	36.9
3	1	1				< 0	44.4
4			1			0.35	25.6
5	1		1			< 0	34.6
6		1	1			0.36	25.8
7	1	1	1			< 0	34.7
8				1		< 0	38.3
9	1			1		< 0	38.9
10		1		1		< 0	37.9
11	1	1		1		< 0	39.1
12		1	1	1		0.28	27.2
13	1		1	1		< 0	36.8
14		1	1	1		0.29	27.3
15	1	1	1	1		< 0	36.8
16					1	0.41	23.9
17	1				1	0.28	27.0
18		1			1	0.40	24.4
19	1	1			1	0.29	27.9
20			1		1	0.74	16.9
21	1		1		1	0.76	15.4
22		1	1		1	0.72	17.6
23	1	1	1		1	0.77	14.4
24				1	1	0.30	26.7
25	1			1	1	0.41	24.7
26		1		1	1	0.29	27.3
27	1	1		1	1	0.39	25.5
28		1	1	1	1	0.75	15.8
29	1		1	1	1	0.75	15.2
30		1	1	1	1	0.73	16.1
31	1	1	1	1	1	0.76	14.8

Fig. 4. Results from leave-one-entire-trial-out cross-validation of total target N rate predictions based on the best predictor set (region, cultivar, Nup$_{zero}$ and yield potential).

region as a predictor for NR$_{target\_trial}$ generally reduced the accuracy of model predictions. Cultivar often had a very small effect on model performance, despite the evident difference in reflectance between cultivars especially in the upper RE and NIR wavelength region (Fig. 3c). The effect of Nup$_{max}$ varied, i.e. it improved predictions when added to
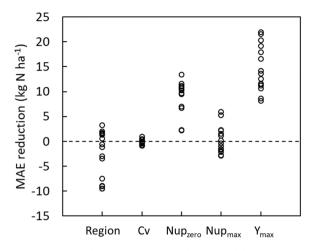
Fig. 5. Importance of the five predictor variables in models for target total N rate. Symbols show the reduction in mean absolute error from adding the predictor to all 15 combinations of the other four predictors. Cv = cultivar; Nup_{zero} = N uptake in zero-plots; Nup_{max} = N uptake in max-plots; Y_{pot} = yield potential.

some predictor sets, but not to others.

3.4. Relative N requirement modelling

Results from the modelling $NR_{sup\_treat\_rel}$ from relative VIs are presented in Fig. 6. In general, multispectral indices performed better than RGB indices. Among the latter, triangular greenness index (TGI) was best-performing (E = 0.58, MAE = 26 kg N ha^{-1}), far better than the three other RGB indices (E $\leq$ 0.18, MAE $\geq$ 41 kg N ha^{-1}). Among the multispectral indices, several performed well, with E values just above 0.8 and MAEs < 20 kg N ha^{-1}. These indices all describe differences in the RE-NIR region, so the best choice for a practical application may depend on considerations other than index performance, such as sensor availability. Scatter plots between predicted and observed values are presented in Fig. 7 for the best-performing RGB index (TGI) and one of the best-performing multispectral indices ($d_{75}r_6$). Model equations for the five best multispectral indices plus the one best RGB index are presented in Table S2 in Supplementary Material.

3.4.1. Absolute remaining N requirement computation

Evaluation metrics for the total supplemental N rate (i.e. the average supplement N rate plus the relative supplement N rate) are presented in Table 6. Scatter plots of predicted versus observed values for NR_{sup_treat} computed from the best NR_{target_trial} model and the models based on these two indices are presented in Fig. 8.
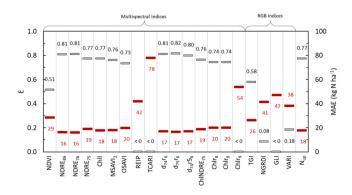

Fig. 6. Evaluation metrics from leave-one-entire-trial-out cross-validation of modelling relative supplemental N rate from relative vegetation index. E = Nash-Sutcliffe modelling efficiency; MAE = mean absolute error.

4. Discussion

4.1. Performance of predictors for total target N rate

The best predictor set for the total target N rate modelling comprised *region, cultivar, Nup_{zero}* and *Y_{pot}*. This supports current best practices in Sweden, where the Swedish Board of Agriculture and advisory organisations recommend adjusting N rates to geographical region, yield potential and N mineralisation level (Swedish Board of Agriculture, 2021). Most agencies also recommend zero-plots as a tool for monitoring current-year N mineralisation (e.g. Rural Economy and Agricultural Societies, 2022). The fertiliser company Yara AB and the Swedish Board of Agriculture have a monitoring programme where N uptake in zero-plots is reported weekly for a number of control plots across Sweden (e.g. through the Focus-on-Nutrients programme; https://greppa.nu/om-greppa-naringen/in-english).

4.2. Performance of vegetation indices

In accordance with earlier studies (e.g. Reusch, 2005), indices based on RE and NIR bands were more efficient in describing the N status of crops than indices based on visible light (Fig. 3). In the present study it was evident the there is also a marked difference in performance between different RGB indices; the validation statistics showed that TGI (E = 0.58; MAE = 26 kg N ha^{-1}) was far better than other indices based on visible light (Fig. 6). According to Hunt et al. (2013), TGI is relatively sensitive to chlorophyll content in the canopy, while being relatively insensitive to leaf area index, which is suitable since predictions of the last supplemental N dose is done late in the season. Several of the RE-NIR indices performed equally well in prediction models for relative NR_{sup_treat} (E: 0.80–0.82; MAE: 16–17 kg N ha^{-1}). These indices were $NDRE_{86}$, $NDRE_{76}$, $d_{75}r_6$, $d_{74}r_6$ and $d_{74}r_{56}$. Band 6 was used for standardisation in all cases. This indicates that band 6 is useful for this purpose, and that band 8 or 7, or the difference between band 7 and band 4, or band 7 and band 5, is useful in combination with band 6. Note that the commonly used normalised difference vegetation index (NDVI) did not perform very well (E = 0.51; MAE = 29 kg N ha^{-1}). The index $MSAVI_2$, which uses the same bands as NDVI, performed better (E = 0.76; MAE = 23 kg N ha^{-1}). If a sensor with only NIR and red bands is available, $MSAVI_2$ would be a better alternative than NDVI for prediction of optimal supplemental N rate in winter wheat at crop development stage DC37.

4.3. Manual, semi-automated or fully automatic DSS

Decision support systems for VRA in N fertilisation can be designed in many ways (e.g. Blondlot et al., 2005; Gutiérrez et al., 2019). A DSS can be fully automatic or require user input in the form of local knowledge and data from handheld sensor measurements in OFE plots. In general, strategies can be considered safer (in terms of N rate accuracy) if some local information is used (Söderström et al., 2017). This can take the form of handheld sensor measurements in the growing crop, or user expert knowledge, e.g. on yield potential of a field or major yield-limiting factors other than N in a field. There is always a risk of a fully automatic system producing severely erroneous N requirement maps if local conditions are not taken into account by the model. A fully manual decision can also generate incorrect recommendations and can be difficult to use (Lundström and Lindblom, 2018). A semi-automated system, using both general relationships between remote-sensing data and crop requirements (built into empirical models), as well as users' tacit knowledge on local conditions that can never be entirely captured by models, is likely a good solution.

4.4. Flexible implementation of the two-step approach

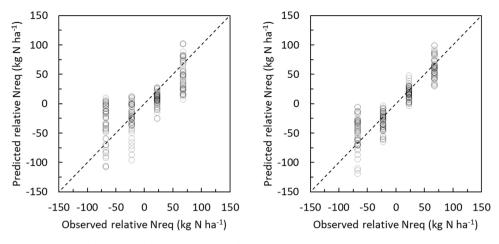A two-step approach was developed for predicting average optimal

Fig. 7. Results from the leave-one-entire-trial-out cross-validation of the modelling relative remaining N requirement from relative vegetation index for two different vegetation indices: a) TGI and b) $d_{75}r_6$.

Table 6

Results of the leave-one-entire-trial-out cross-validations of the absolute supplemental N rate N requirement (NR$_{sup\_treat}$) modelling. Validation metrics are presented for the best RGB index (TGI) and the best multispectral index ($d_{75}r_6$) for 31 predictor sets. The predictor set numbers are the same as in Table 5. Evaluation metrics for the leave-one-entire-trial-out cross-validation of target total N rate models for 31 predictor sets (combination of region, cultivar, N uptake in zero-plots (Nupzero), N uptake in max-plots (Nupmax), and yield potential (Ypot)). The number 1 indicates inclusion in the predictor set. E = Nash-Sutcliffe modelling efficiency; MAE = mean absolute error.

Predictor set	E (TGI)	MAE (TGI) (kg N ha^{-1})	E ($d_{75}r_6$)	MAE ($d_{75}r_6$) (kg N ha^{-1})
4	0.54	23.0	0.62	20.6
6	0.54	23.0	0.62	20.7
12	0.51	23.7	0.59	21.6
13	0.33	28.9	0.40	27.3
14	0.51	23.7	0.59	21.7
16	0.64	21.0	0.70	18.2
17	0.56	23.1	0.64	20.4
18	0.62	22.0	0.68	19.1
19	0.54	24.1	0.62	21.2
20	0.72	17.6	0.80	14.5
21	0.74	16.6	0.82	13.4
22	0.70	18.4	0.78	15.4
23	**0.74**	**16.7**	**0.82**	**13.5**
24	0.62	21.6	0.68	19.0
25	0.60	21.6	0.71	18.5
26	0.60	22.5	0.65	19.8
27	0.58	22.5	0.69	19.4
28	0.72	17.7	0.80	14.3
29	0.74	17.1	0.81	13.9
30	0.70	18.5	0.78	15.1
31	0.74	17.2	0.81	14.1

supplemental N rate in a field or a management zone and then further adapting the N rate at finer spatial scale in relation to the current N status of the crop in a DSS. The approach is flexible, as the two prediction models can be used individually or in combination (Fig. 9). For example, an alternative to using the NR$_{target\_trial}$ model, an expert assessment of optimal total supplemental N rate can be made or, regional recommendations from advisory services can be used. The N rate could then be varied within the field or the zone according to the VI-based model for relative supplemental N rate. This is how tractor-borne sensors for VRA of N often work. The NR$_{target\_trial}$ prediction model could also be used separately to determine NR$_{target\_trial}$ per field or management zone, and then apply a uniform N rate within that field or the zone or vary the N rate based on a tractor-borne sensor.

4.5. Remaining challenges in streamlining a functional DSS for VRA of N

Implementation of remote sensing-based prediction models of optimal supplemental N rate in a DSS, can enable wider adoption of precision N management, and consequently better N fertilizer use efficiency. We have identified ten aspects that must be considered to streamline a functional DSS with continuous model updating. Some of the challenges are further discussed in the following sections.

1. *Designing national field trial series to produce data for model calibration.* National field trials are usually carried out in locations with favourable conditions for crop growth and cannot be considered representative for areas with poorer cropping conditions. There is an urgent need for new field trial designs that produce calibration data for models predicting within-field variation in crop nutrient requirements.
2. *Designing on-farm experiments to produce data for model application.* Experiments (number, size and locations of plots) must be representative for an entire farm, field or subfield zone, and suit the mode of data collection (proximal or remote sensor). These trials may or may not be the same as the ones in the previous point (see further discussion in Section 4.6).
3. *Handling yield-limiting factors other than nitrogen.* One strategy could be to, like in the intended application of the present study, work with homogeneous zones (i.e zones that are homogeneous in all other yield limiting factors than the level of plant available N). A lot of research has been conducted on how to split fields into management zones but to make the present modelling framework applicable in practice, functionality for this also needs to be implemented in a DSS and that requires the zoning-algorithm to be based on spatial data suitable for this purpose. An alternative option could be to work with spatially continuous data on yield potential.
4. *Handling model sensitivity to crop developmental stage.* If one would choose to directly predict absolute optimal supplemental N rate based on reflectance data from remote sensing (instead of relative supplemental N rate as done in the present study), one would need to apply the model on data from the specific crop developmental stage for which they were calibrated. However, satellite data may not always be available for all developmental stages and it may be difficult for the user to know the exact developmental stage of the crop. In a DSS, however, the user can be assisted with predictions of crop developmental stage. Crop phenology can be forecasted using mechanistic (Ceglar et al., 2019; Nutini et al., 2021) or empirical (McMaster and Smika, 1988; Wolters, 2022) models.
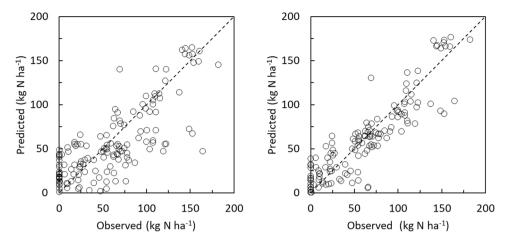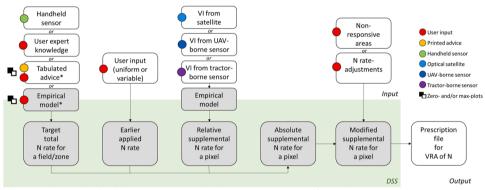
Fig. 8. Results from the leave-one-entire-trial-out cross-validation of total supplemental N rate, computed from the best total target N rate model (predictors: region, cultivar, N uptake in zero-plots and yield potential) and two models for relative supplemental N rate based on: a) TGI (best RGB index), and b) $d_{75}r_6$ (best multi-spectral index).

Fig. 9. Suggested implementation of the models in a decision support system (DSS) with indications of required input. VI = vegetation index; VRA = variable rate application.

5. *Optimising N rate with respect to multiple goals.* A procedure that simultaneously optimises N rate with respect to profit, grain protein goals, nutrient use efficiency and risk for lodging remains (to our knowledge) to be developed (see further discussion in Section 4.7).

6. *Growth conditions in the remainder of the season are unknown at the time of supplemental fertilisation.* This is a (perhaps forever-unavoidable) source of uncertainty in supplemental N rate decision.

7. *Ensuring robust model.* Development of models that perform well at sites and years other than those used for model parameterisation requires extensive datasets for calibration, plus a validation approach that assesses model performance for new sites and years.

8. *Ensuring up-to-date models.* Modelling frameworks can be general, but models are specific. It should be possible to develop functional principles for modelling that can be widely adopted and used for a long time, but the model will always be specific and would need to be updated for new cultivars, sensors and geographical areas.

9. *Handling measurement sensitivity to ambient light conditions and soil reflectance.* Crop canopy reflectance measurements are sensitive to ambient light conditions and soil reflectance. Some current remedies are: use of reflectance panels and/or incoming light sensors for data corrections, use of vegetation indices rather than reflectance values and modelling relative rather than absolute

values of crop properties (e.g. relative remaining N requirement within a field) (see further discussion in Section 4.8).

10. *Handling model sensitivity to optical sensor and platform.* The error introduced when applying a model parameterised with data from one system (e.g. a UAV-borne camera) to data from another system (e.g. a satellite mission) is unknown. Further investigations, possibly on the potential to use platform-transfer functions for co-calibration of different sensors, are needed (see further discussion in Section 4.9).

4.6. Design of miniature on-farm experiments

Conventional replicated full-factorial small-plot trials (as used here) are commonly used for agronomic research, and for development of recommendations to farmers. To overcome some of the limitations in transferring results to farmers' fields, on-farm experimentation (OFE) is suggested to provide information that better supports on-farm decisions (Lacoste et al., 2022). On-farm experiments in the form of zero-plots and/or max-plots (or strips) can provide excellent local and current information on soil N supply and yield potential (e.g. Johnson and Raun, 2003), and the present study confirms their usefulness in modelling of optimal supplemental N rate in winter wheat. There are a number of interlinked considerations when designing small OFEs, including where to place the plots, how many plots are needed, how big does the plot have to be, and how to collect data. It is labour-intensive to make handheld measurements at several locations in (often) several fields. For handheld (or potentially UAV-borne) sensor measurements, relatively

small plots (~10 m^2) are sufficient in principle. Alternatively, satellite data can be used, but with current satellites much larger plots would be required. Farmers using boom spreaders can easily generate both zero-plots and max-plots, whereas users of the more common disc spreader must protect areas with tarpaulin to generate a small zero-plot. Using max-plots may be easier and also cheaper, since there is no yield loss, only an extra cost for the super-optimal N fertiliser, but they were demonstrated less useful for sole use than zero-plots in the present study. It can be mentioned in this context that even simpler local information sources than OFEs have been proposed. For example, Holland and Schepers (2013) suggested to use "virtual reference" areas in a field with statistically confirmed adequate supply of N, instead of established max-plots.

4.7. Optimising N rate with respect to multiple goals

There are many aspects to consider when determining supplementary N rate, but it is commonly optimised with respect to profit. If the aim is to achieve a target grain protein concentration, it may be necessary to increase the N rate. On the other hand, to decrease the risk of lodging and N losses to the environment by nitrate leaching and nitrous oxide emissions, it may be necessary to lower the N rate. In this study, mean protein content at target total N rate was 10.4% and, on average, an additional 18 kg N ha^{-1} was needed to reach a grain protein concentration of 11.5% (not shown), although there was a large variation between cultivars (Etana 7 kg N ha^{-1}, Hallfreda 44 kg N ha^{-1}, Informer 27 kg N ha^{-1}, Julius 8 kg N ha^{-1}, RGT Reform 13 kg N ha^{-1}). N use efficiency (here calculated as harvested N in grain/N applied) was 87% at NR$_{target\_trial}$, with a standard deviation of 19 percentage points. The amount of non-harvested N increased relatively rapidly when total N rate exceeded 130 kg N per ha (Fig. 10).

4.8. Data collection challenges

Data from remote reflectance measurements of field crops will be affected by the ambient light conditions, such as photon flux density, spectral distribution of the incoming light and solar elevation angle, but also by soil reflectance if the canopy is not closed. In this study, data collection was done under somewhat varying weather conditions and at different times of the day (see Fig. 1). It is difficult to avoid this type of variation when data collection must be made at a specific crop development stage, and when the data collection method (UAV flights) itself has restrictions in terms of weather (days with rain and hard winds are excluded). An additional challenge was that some sites were located close to airports, which ban UAV flights except in certain narrow time slots. The effects of these factors are somewhat different in different wavelength bands, with RE-NIR indices reported to be less sensitive to solar elevation angle differences (de Souza et al., 2021).

4.9. Model sensitivity to optical sensor and platform

In the present study, it is assumed that models calibrated with spectral measurements from UAV-borne remote sensing can be directly applied on Sentinel-2 data, since the spectral specifications of the sensors are similar. Previous comparisons of indices derived from UAV-borne sensors and Sentinel-2 data, e.g. by Peng et al. (2021), Bukowiecki et al. (2021), Rasmussen et al. (2020) and Söderström et al. (2021), have shown that the results depend on the approach used and
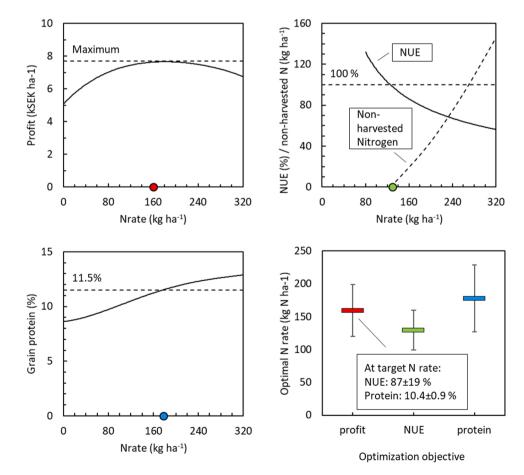

Fig. 10. Average curves for profit, nitrogen use efficiency (NUE), and amount of non-harvested N and grain protein concentration in relation to N rate (fitted to all data in the study). Target total N rate = optimal nitrogen rate as determined in this study (i.e. optimal with respect to profit when the price ratio is 10 kg grain per kg N).

the index. Relative variation seems to be easier to reproduce than exact index values (Söderström et al., 2021), indicating that models based on relative variation may be more robust than models based on absolute VI values. In addition to the unknown accuracy issues with transfer between platforms, there are also difficulties in managing data from UAVs (Maes and Steppe, 2019; this study), and data quality may differ over time because of manual calibration procedures etc. On the other hand, satellite data are not entirely consistent and subtle shifts in georeferencing and atmospheric conditions may have considerable effects on outputs, especially for precision agricultural applications that use such data at more or less pixel level. In addition, cloud-free images for the crop developmental stage of interest may not be available. Continued streamlining of the process to collect and prepare UAV data may be the best way forward, or it might be better to adapt the designs and geometries of field trials to match satellite data. Again, this calls for new field trial designs, an integral component in the ongoing development of OFE (Lacoste et al., 2021).

5. Conclusions

In the present study:

- It proved possible to predict optimal total N rate for new sites and years with an MAE of 14 kg N ha^{-1} (model based on region, cultivar, Nup$_{zero}$ and Y$_{pot}$). Relative remaining N requirement could be predicted with an MAE of 17 kg N ha^{-1} (model based on the VI d$_{75}$r$_6$). The supplemental N rate to apply, computed from predictions by these two models, plus the N rate earlier in the season, had an MAE of 14 kg N ha^{-1}. The most important predictors for optimal total N rate were Y$_{pot}$ and Nup$_{zero}$. Multispectral indices worked better than RGB indices.
- The correlation between optimal supplemental N rate (which is also a measure of crop N status) and crop canopy reflectance was strongest for bands 3, 5, 7, 8 and 8A (negative for bands 3 and 5, positive in the NIR wavelength region) and weakest for band 6.
- Semi-automatic DSS have the great advantages of *i*) utilising farmers' tacit knowledge on local conditions better than fully automatic DSS and *ii*) making use of information from field trials (captured by models) and remote-sensing data better than fully manual decisions.

CRediT authorship contribution statement

Kristin Piikki: Conceptualisation, Methodology, Investigation, Formal analyses, Writing – original draft preparation, Writing – review & editing. **Mats Söderström**: Conceptualisation, Methodology, Investigation, Writing – original draft preparation, Writing – review & editing. **Henrik Stadig**: Conceptualisation, Methodology, Writing – review & editing.

Declaration of Competing Interest

The authors declare that they have no known competing financial interests or personal relationships that could have appeared to influence the work reported in this paper.

Data availability

The authors are unable or have chosen not to specify which data has been used.

Acknowledgements

Competing interests statement

The authors have no competing interests to declare.

Appendix A. Supporting information

Supplementary data associated with this article can be found in the online version at doi:10.1016/j.fcr.2022.108742.

References

Ali, M.M., Al-Ani, A., Eamus, D., Tan, D.K., 2017. Leaf nitrogen determination using non-destructive techniques–A review. J. Plant Nutr. 40 (7), 928–953. https://doi.org/10.1080/01904167.2016.1143954.

Alshihabi, O., Piikki, K., Söderström, M., 2019. CropSAT–a decision support system for practical use of satellite images in precision agriculture. In International Conference on Smart Information & Communication Technologies. Springer,, Cham, pp. 415–421. https://doi.org/10.1007/978-3-030-53187-4_45.

Bannari, A., Morin, D., Bonn, F., Huete, A.R., 1995. A review of vegetation indices. Remote Sens. Rev. 13 (1), 95–120. https://doi.org/10.1080/02757259509532298.

Barnes, E.M., Clarke, T.R., Richards, S.E., Colaizzi, P.D., Haberland, J., Kostrzewski, M., & Moran, M.S. (2000, July). Coincident detection of crop water stress, nitrogen status and canopy density using ground based multispectral data. In Proceedings of the Fifth International Conference on Precision Agriculture: Bloomington, MN, USA.

Blondlot, A., Gate, P., Poilve, H., 2005. Providing operational nitrogen recommendations to farmers using satellite imagery. Precision Agriculture '05. Wageningen Academic Publishers,, Wageningen, pp. 345–352.

Bukowiecki, J., Rose, T., Kage, H., 2021. Sentinel-2 Data for Precision Agriculture? –A UAV-Based Assessment. Sensors 21 (8), 2861. https://doi.org/10.3390/s21082861.

Ceglar, A., Van der Wijngaart, R., De Wit, A., Lecerf, R., Boogaard, H., Seguini, L., Baruth, B., 2019. Improving WOFOST model to simulate winter wheat phenology in Europe: Evaluation and effects on yield. Agric. Syst. 168, 168–180. https://doi.org/10.1016/j.agsy.2018.05.002.

Chen, P., 2015. A comparison of two approaches for estimating the wheat nitrogen nutrition index using remote sensing. Remote Sens. 7 (4), 4527–4548. https://doi.org/10.3390/rs70404527.

Delin, S., & Stenberg, M. (2012). Nitratutlakning beroende på kvävegödslingsnivå och skörderespons i havre på en lätt jord (Nitrate leaching depending on nitrogen fertilisation and yield response in oat on a sandy soil). Dept of Soil and Environment, Swedish University of Agriculutral Sciences, SLU. Report 10, Uppsala, Sweden. Available at: ⟨https://pub.epsilon.slu.se/9099/1/delin_s_120927.pdf⟩ (Accessed: March 1, 2022).

European Parliament, 2019, Precision agriculture and the future of farming in Europe: scientific foresight study. https://doi.org/10.2861/175493.

FAO, 2017. The Future of Food and Agriculture. Trends and Challenges. Food and Agriculture Organization of the United Nations,, Rome (Available at). ⟨https://www.fao.org/3/i6583e/i6583e.pdf⟩.

FAO, 2019. The International Code of Conduct for the Sustainable Use and Management of Fertilizers. Food and Agriculture Organization of the United Nations,, Rome (Available at). ⟨https://www.fao.org/3/ca5253en/ca5253en.pdf⟩.

Gitelson, A.A., Kaufman, Y.J., Stark, R., Rundquist, D., 2002. Novel algorithms for remote estimation of vegetation fraction. Remote Sens. Environ. 80 (1), 76–87. https://doi.org/10.1016/S0034-4257(01)00289-9.

Gitelson, A.A., Gritz, Y., Merzlyak, M.N., 2003. Relationships between leaf chlorophyll content and spectral reflectance and algorithms for non-destructive chlorophyll assessment in higher plant leaves. J. Plant Physiol. 160 (3), 271–282. https://doi.org/10.1078/0176-1617-00887.

Gutiérrez, F., Htun, N.N., Schlenz, F., Kasimati, A., Verbert, K., 2019. A review of visualisations in agricultural decision support systems: An HCI perspective. Comput. Electron. Agric. 163, 104844 https://doi.org/10.1016/j.compag.2019.05.053.

Guyot, G., Baret, F., Major, D.J., 1988. High spectral resolution: determination of spectral shifts between the red and the near-infrared. Int. Arch. Photogramm. Remote Sens. Spat. Inf. Sci. 11, 750–760.

Haboudane, D., Miller, J.R., Tremblay, N., Zarco-Tejada, P.J., Dextraze, L., 2002. Integrated narrow-band vegetation indices for prediction of crop chlorophyll content for application to precision agriculture. Remote Sens. Environ. 81 (2–3), 416–426. https://doi.org/10.1016/S0034-4257(02)00018-4.

Holland, K.H., Schepers, J.S., 2013. Use of a virtual-reference concept to interpret active crop canopy sensor data. Precis. Agric. 14 (1), 71–85. https://doi.org/10.1007/s11119-012-9301-6.

Huete, A.R., 1988. A soil-adjusted vegetation index (SAVI. Remote Sens. Environ. 25 (3), 295–309. https://doi.org/10.1016/0034-4257(88)90106-X.

Hunt Jr, E.R., Doraiswamy, P.C., McMurtrey, J.E., Daughtry, C.S., Perry, E.M., Akhmedov, B., 2013. A visible band index for remote sensing leaf chlorophyll

content at the canopy scale. Int. J. Appl. Earth Obs. Geoinf. 21, 103–112. https://doi.org/10.1016/j.jag.2012.07.020.

International Society of Precision Agriculture, 2018, Precision ag definition. Available at: ⟨https://www.ispag.org/about/definition⟩ (Accessed: March 1, 2022).

IPCC, 2019, Climate Change and Land: an IPCC special report. Available at: ⟨https://bit.ly/3oTlmAd⟩ (Accessed: March 1, 2022).

Johnson, G.V., Raun, W.R., 2003. Nitrogen response index as a guide to fertilizer management. J. Plant Nutr. 26 (2), 249–262. https://doi.org/10.1081/PLN-120017134.

Kim, M.S., Daughtry, C.S.T., Chappelle, E.W., McMurtrey, J.E., & Walthall, C.L. (1994). The use of high spectral resolution bands for estimating absorbed photosynthetically active radiation (A par). In CNES, proceedings of 6th international symposium on physical measurements and signatures in remote sensing (No. GSFC-E-DAA-TN72921). p. 299–306.

Kottek, M., Grieser, J., Beck, C., Rudolf, B., Rubel, F., 2006. World Map of the Köppen-Geiger climate classification updated. Meteorol. Z. 15 (3), 259–263. https://doi.org/10.1127/0941-2948/2006/0130.

Lacoste, M., Cook, S., McNee, M., et al., 2022. On-Farm Experimentation to transform global agriculture. Nat. Food 3, 11–18. https://doi.org/10.1038/s43016-021-00424-4.

Louhaichi, M., Borman, M.M., Johnson, D.E., 2001. Spatially located platform and aerial photography for documentation of grazing impacts on wheat. Geocarto Int. 16 (1), 65–70. https://doi.org/10.1080/10106040108542184.

Lundström, C., Lindblom, J., 2018. Considering farmers' situated knowledge of using agricultural decision support systems (AgriDSS) to Foster farming practices: The case of CropSAT. Agric. Syst. 159, 9–20. https://doi.org/10.1016/j.agsy.2017.10.004.

Maes, W.H., Steppe, K., 2019. Perspectives for remote sensing with unmanned aerial vehicles in precision agriculture. Trends Plant Sci. 24 (2), 152–164. https://doi.org/10.1016/j.tplants.2018.11.007.

McMaster, G.S., Smika, D.E., 1988. Estimation and evaluation of winter wheat phenology in the central Great Plains. Agric. For. Meteorol. 43 (1), 1–18. https://doi.org/10.1016/0168-1923(88)90002-0.

Nash, J.E., Sutcliffe, J.V., 1970. River flow forecasting through conceptual models part I—A discussion of principles. J. Hydrol. 10 (3), 282–290. https://doi.org/10.1016/0022-1694(70)90255-6.

Nocerino, E., Dubbini, M., Menna, F., Remondino, F., Gattelli, M., Covi, D., 2017. Geometric calibration and radiometric correction of the MAIA multispectral camera. Int. Arch. Photogramm., Remote Sens. Spat. Inf. Sci. 42. https://doi.org/10.5194/isprs-archives-XLII-3-W3-149-2017.

Nutini, F., Confalonieri, R., Crema, A., Movedi, E., Paleari, L., Stavrakoudis, D., Boschetti, M., 2018. An operational workflow to assess rice nutritional status based on satellite imagery and smartphone apps. Comput. Electron. Agric. 154, 80–92. ⟨https://linkinghub.elsevier.com/retrieve/pii/S0168⟩.

Nutini, F., Confalonieri, R., Paleari, L., Pepe, M., Criscuolo, L., Porta, F., Ranghetti, R., Busetto, L., Boschetti, M., 2021. Supporting operational site-specific fertilisation in rice cropping systems with infield smartphone measurements and Sentinel-2 observations. Precis. Agric. 22 (4), 1284–1303. https://doi.org/10.1007/s11119-021-09784-0.

Peng, J., Manevski, K., Kørup, K., Larsen, R., Andersen, M.N., 2021. Random forest regression results in accurate assessment of potato nitrogen status based on multispectral data from different platforms and the critical concentration approach. Field Crops Res. 268, 108158 https://doi.org/10.1016/j.fcr.2021.108158.

Piikki, K., Söderström, M., 2019. Digital soil mapping of arable land in Sweden–Validation of performance at multiple scales. Geoderma 352, 342–350. https://doi.org/10.1016/j.geoderma.2017.10.049.

Piikki, K., Stenberg, B., 2017.). A modified delta yield approach for estimation of economic optimal nitrogen rate (EONR) for wheat (*Triticum aestivum* L.) and barley (*Hordeum vulgare* L.). Agric. Food Sci. 26 (4), 233–241. https://doi.org/10.23986/afsci.63668.

Piikki, K., Wetterlind, J., Söderström, M., & Stenberg, B., 2021, Notes on the valmetrics package. Available at: ⟨https://cran.r-project.org/web/packages/valmetrics/vignettes/notes.html⟩ (Accessed: March 1, 2022).

Pretty, J., Bharucha, Z.P., 2014. Sustainable intensification in agricultural systems. Ann. Bot. 114 (8), 1571–1596. https://doi.org/10.1093/aob/mcu205.

Qi, J., Chehbouni, A., Huete, A.R., Kerr, Y.H., Sorooshian, S., 1994. A modified soil adjusted vegetation index. Remote Sens. Environ. 48 (2), 119–126. https://doi.org/10.1016/0034-4257(94)90134-1.

R Core Team, 2021, R: A language and environment for statistical computing. R Foundation for Statistical Computing, Vienna, Austria. Available at: ⟨https://www.R-project.org/⟩ (accessed 1 March 2022).

Rasmussen, J., Azim, S., Kjærgaard Boldsen, S., Nitschke, T., Jensen, S.M., Nielsen, J., Christensen, S., 2020. The challenge of reproducing remote sensing data from satellites and unmanned aerial vehicles (UAVs) in the context of management zones and precision agriculture. Precis. Agric. 22, 834–851. https://doi.org/10.1007/s11119-020-09759-7.

Raun, W.R., Johnson, G.V., 1999. Improving nitrogen use efficiency for cereal production. Agron. J. 91 (3), 357–363. https://doi.org/10.2134/agronj1999.00021962009100030001x.

Raun, W.R., Solie, J.B., Johnson, G.V., Stone, M.L., Lukina, E.V., Thomason, W.E., Schepers, J.S., 2001. In-season prediction of potential grain yield in winter wheat using canopy reflectance. Agron. J. 93 (1), 131–138. https://doi.org/10.2134/agronj2001.931131x.

Reusch, S., 2003, Optimisation of oblique-view remote measurement of crop N-uptake under changing irradiance conditions. In Precision agriculture: Papers from the 4th European Conference on Precision Agriculture: Wageningen Academic Publishers. p. 573–578.

Reusch, S., 2005. Optimum waveband selection for determining the nitrogen uptake in winter wheat by active remote sensing. Precision Agriculture '05. Wageningen Academic Publishers,, Wageningen, pp. 261–266.

Rondeaux, G., Steven, M., Baret, F., 1996. Optimization of soil-adjusted vegetation indices. Remote Sens. Environ. 55 (2), 95–107. https://doi.org/10.1016/0034-4257(95)00186-7.

Rouse Jr, J.W., Haas, R.H., Schell, J.A., & Deering, D.W. (1973). Monitoring the vernal advancement and retrogradation (green wave effect) of natural vegetation (No. NASA-CR-132982). Available at: ⟨https://ntrs.nasa.gov/api/citations/19730017588/downloads/19730017588.pdf⟩ (Accessed: March 1, 2022).

Söderström, M., Piikki, K., Stenberg, M., Stadig, H., Martinsson, J., 2017. Producing nitrogen (N) uptake maps in winter wheat by combining proximal crop measurements with Sentinel-2 and DMC satellite images in a decision support system for farmers. Acta Agric. Scand., Sect. B—Soil Plant Sci. 67 (7), 637–650. https://doi.org/10.1080/09064710.2017.1324044.

Söderström, M., Piikki, K., Stadig, H., 2021. Yield maps for everyone - scaling drone models for satellite-based decision support. In Precision Agriculture '21. Wageningen Academic Publishers,, Wageningen, the Netherlands, pp. 911–918. https://doi.org/10.3920/978-90-8686-916-9_109.

de Souza, R., Buchhart, C., Heil, K., Plass, J., Padilla, F.M., Schmidhalter, U., 2021. Effect of Time of Day and Sky Conditions on Different Vegetation Indices Calculated from Active and Passive Sensors and Images Taken from UAV. Remote Sens. 13 (9), 1691. https://doi.org/10.3390/rs13091691.

Swedish Board of Agriculture, 2021, Rekommendationer för gödsling och kalkning 2022 (Recommendations for fertilisation and liming 2022). Report JO21:9: Jordbruksverket, Jönköping, Sweden. Available at: ⟨https://www2.jordbruksverket.se/download/18.48cc999c17f29af389d21875/1645717319949/jo21_9.pdf⟩ (Accessed: March 1, 2022). in Swedish.

Vizzari, M., Santaga, F., Benincasa, P., 2019. Sentinel 2-based nitrogen VRT fertilisation in wheat: Comparison between traditional and simple precision practices. Agronomy 9 (6), 278. https://doi.org/10.3390/agronomy9060278.

Wolters, S., 2022, Towards synthesis for nitrogen fertilisation using a decision support system. Acta Agriculturae Sueciae 2022:59. Doctoral thesis available at: ⟨https://pub.epsilon.slu.se/28958/⟩ (accessed 19 October 2022).

Wolters, S., Söderström, M., Piikki, K., Reese, H., Stenberg, M., 2021. Upscaling proximal sensor N-uptake predictions in winter wheat (*Triticum aestivum* L.) with Sentinel-2 satellite data for use in a decision support system. Precis. Agric. 22 (4), 1263–1283. https://doi.org/10.1007/s11119-020-09783-7.

Wolters, S., Söderström, M., Piikki, K., Börjesson, T., Pettersson, C.G., 2022. Predicting grain protein concentration in winter wheat (*Triticum aestivum* L.) based on unpiloted aerial vehicle multispectral optical remote sensing. Acta Agric. Scand., Sect. B — Soil Plant Sci. 72 (1), 788–802. https://doi.org/10.1080/09064710.2022.2085165.

Zadoks, J.C., Chang, T.T., Konzak, C.F., 1974. A decimal code for the growth stages of cereals. Weed Res. 14 (6), 415–421. https://doi.org/10.1111/j.1365-3180.1974.tb01084.x.